



Development of In-House Coaxial Thermocouples and Their Calibration

Dániel G. Kovács! Sebastien Paris? Guillaume Grossir3

Abstract

This work focuses on developing in-house manufacturing and calibration techniques for coaxial thermocouples, aiming to measure transient surface temperatures and infer wall heat fluxes within shortduration hypersonic facilities. A furnace-based oxidation technique is tested to electrically insulate and mount a Chromel tube and a Constantan bar together, creating an E-type coaxial thermocouple. Successful bonding and electrical insulation between the two materials are demonstrated, and the active junction of the thermocouple is effectively obtained by scratching the oxidized surfaces. Design and manufacturing recommendations are issued and are expected to reduce the insulation layer thickness between the materials and to shorten the response time of the sensor. A liquid droplet dripping-based calibration methodology is established to measure the thermal product of such thermocouples. A parametric study addresses the influence of droplet size, dripping height, and droplet viscosity on the response of the thermocouple and on the corresponding thermal product.

Keywords: hypersonics, ground testing, measurement techniques, coaxial thermocouple, heat-flux sensor

Nomenclature

Latin

C – specific heat, $\frac{J}{ka}$

D – diameter, m h - height, m

k – specific heat, $\frac{W}{mK}$

L – length, m \dot{q} – heat-flux, $\frac{\mathrm{W}}{\mathrm{m}^2}$

S – surface, m^2 t – time, s

T – temperature, K

 α — thermal diffusivity, $\frac{m^2}{s}$ β — thermal product, $\frac{J}{m^2K\sqrt{s}}$

 δ – thermal penetration depth, mm

 μ – dynamic viscosity, Pa.s

 ρ – density, $\frac{kg}{m^3}$

 σ – standard deviation, –

Subscripts

0 - condition at initial state

1 - body 1

2 - body 2

amb - ambient

c - contact

Chr - Chromel

Con - Constantan

G – glycerin

L – large droplet

min - minimum

ref - reference

s – surface

S - small droplet

W - water

1. Introduction

Coaxial thermocouples are robust, fast-response transducers aiming at the measurement of transient surface temperatures, which can allow the assessment of the corresponding wall heat flux. Such ther-

¹von Karman Institute for Fluid Dynamics, Waterloosesteenweg 72, B-1640, Sint-Genesius-Rode, Belgium, daniel.gabor.kovacs@vki.ac.be

²von Karman Institute for Fluid Dynamics, Waterloosesteenweg 72, B-1640, Sint-Genesius-Rode, Belgium, sebastien.paris@vki.ac.be

³von Karman Institute for Fluid Dynamics, Waterloosesteenweg 72, B-1640, Sint-Genesius-Rode, Belgium, guillaume.grossir@vki.ac.be

mocouples also operate on the thermoelectric principle as the conventional wire-based configurations, but their structure is different. According to the design proposed by Bendersky (1953), one element is nested inside the other coaxially. A thin layer of insulation separates the two materials along the cylindrical surface, which is bridged by metallic flakes forming the sensing junctions at the sensor's tip. These tiny, sensitive elements are located over the circular circumference of the insulation layer separating the two metals and have low thermal inertia, which contributes to fast responsiveness in the order of a few microseconds. Figure 1 illustrates the classic structure of a K-type (Chromel – Alumel) coaxial thermocouple and a microscopic view of the typical surface junctions. As opposed to platinum thin-film and fine-wire thermocouples, which may require frequent replacement or reinstallation due to the abrasion of the flow (Mohammed et al., 2008), the coaxial sensors are rugged, and the sensing junctions can be easily refurbished by scratching the surface of the thermocouple with a scalpel or sandpaper if necessary.

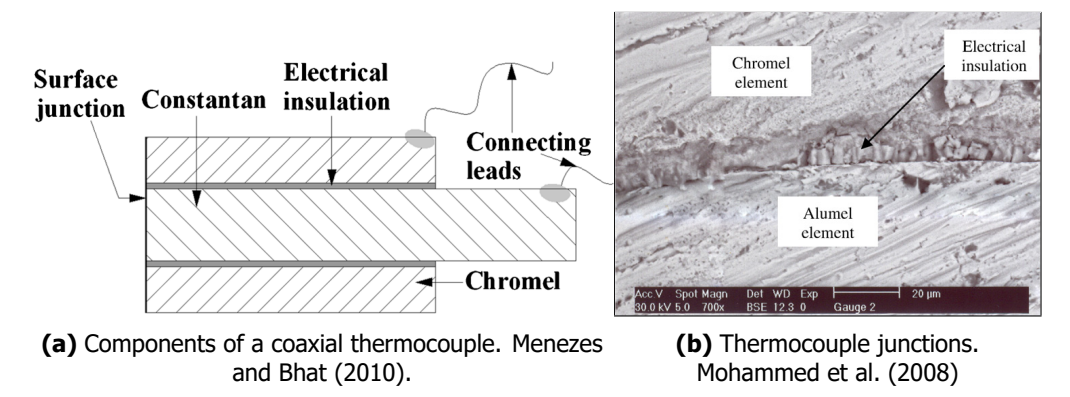


Fig 1. Basic schematic of a coaxial thermocouple.

Coaxial thermocouples can be used to infer the transient wall heat-flux from the measurement of the surface temperature history (Schultz and Jones, 1973) according to:

$$\dot{q}_{s} = \frac{\beta}{\sqrt{\pi}} \left(\frac{T_{s}(t) - T_{0}}{\sqrt{t}} + \frac{1}{2} \int_{0}^{t} \frac{T_{s}(t) - T_{s}(\tau)}{\sqrt{t - \tau}} d\tau \right) \tag{1}$$

where \dot{q}_s is the wall heat-flux, β is the thermal product of the thermocouple, $T_s(t)$ is the surface temperature, and T_0 is the initial temperature; subject to the fulfillment of the following assumptions and requirements: 1) the heat-flux is one-dimensional, along the sensor's axis; 2) the coaxial thermocouple can be considered as a semi-infinite solid body, i.e., the thermal penetration depth (δ) is less than the thickness of the substrate (Schultz and Jones, 1973); 3) the thermal properties are uniform and constant. Major parameters for heat-flux measurement are the transducer's thermal product:

$$\beta = \sqrt{\rho c k} \quad , \tag{2}$$

where ρ is density, c is heat capacity, and k is thermal conductivity of the sensing junctions, and the thermal penetration depth:

$$\delta \approx 4\sqrt{\alpha t} = 4\sqrt{\frac{k}{\rho c}t}$$
 , (3)

which constrains the maximum useful measurement duration (Schultz and Jones, 1973). For the practical use of these thermocouples, different types of calibrations must be performed to identify their sensitivity (temperature - voltage relationship), response time, and thermal product.

The ruggedness and the fast response offered by these sensors make them well-suited for transient temperature measurements. They have been extensively employed within short-duration supersonic

and hypersonic facilities, e.g., shock tubes, shock tunnels (Surujhlal et al., 2023), gun tunnels (Grossir et al., 2019), Ludwieg tubes (Juliano et al., 2015), etc., as well as during flight experiments (Wheaton and Dufrene, 2024). The objective of this work is to establish in-house manufacturing capabilities for coaxial thermocouples and to develop procedures for the calibration of their thermal parameters. This paper summarizes the current work towards an efficient and robust manufacturing capability and on the development of a test methodology for the calibration of the thermal product.

The paper is structured as follows. Section 2 reviews the design and manufacturing techniques of coaxial thermocouples. Section 3 introduces the design chosen for the in-house sensor, and Section 4 presents the initial efforts on its manufacturing using a furnace. Section 5 focuses on the second aspect of this work, the calibration of the thermal product, and presents a test bench and a parametric study executed on a commercial transducer to identify the optimal setup properties. Finally, Section 6 concludes the work accomplished and presents the next steps of the research.

2. Review of coaxial thermocouple design and manufacturing

2.1. Material

In the case of thermocouples, depending on the materials applied, Iron-Constantan, Chromel-Alumel, Copper-Constantan etc., respectively J-type, K-type, T-type etc. thermocouple junctions can be created. The arrangement of the elements (inner and outer), depends on the electrode potential of the materials. The material with the higher electrode potential is always used as an outer element. As Chromel – Constantan thermocouples have the highest thermoelectric sensitivity, the elements have similar thermal properties and have high resistance against corrosion, the corresponding E-type configuration is used in this work. Chromel is used as the outer element, and Constantan is used as the inner component.

2.2. Geometry

The design of these sensors may slightly vary from the one shown in Fig. 1 in order to support their manufacturing process, but the main schematic remains the same. Buttsworth (2001), Mohammed et al. (2008), Menezes and Bhat (2010) and Li et al. (2017) used cylindrical geometries. The advantage of this method is in its simplicity; in case of erosion of the surface junctions, a small piece of the sensor can be cut off, and the contacts can be easily refurbished due to the even distance between the inner and the outer element.

Marineau and Hornung (2009) and Desikan et al. (2016) used a refined design, where the inner element has a conic part, which centralizes it from one side during the assembly. Afterwards, the out-hanging parts are being machined and the junctions can be formed similarly to the aforementioned case. The machining of the taper is very crucial; in case of a too wide angle, the gap between the elements can idneed become bridgeless. Moreover, as the thermocouple erodes and the surface needs to be polished and rescratched, the increasing gap between the elements can become cumbersome to overarch due to the large taper angle, and adversely impact the response time of the sensor.

2.3. Insulation layer and assembly

For the insulation between the thermocouple elements, Bendersky (1953) used an aluminum oxide layer on the surface of the inner material. Buttsworth and Jacobs (1998) also succeeded in using surface oxidation for insulation; a 6-hour-long $1000\,^{\circ}\text{C}$ furnace program resulted in the formation of a $20\,\mu\text{m}$ oxide layer and the bonding of the pre-assembled K-type thermocouple elements. In more recent works (Marineau and Hornung, 2009; Mohammed et al., 2010; Menezes and Bhat, 2010; Desikan et al., 2016), the isolation and assembly was more favorably created by a thin layer of epoxy. Park et al. (2024) noted that if the thermocouple elements are oxidized separately, the insulation layer may get damaged during the assembly process (resulting in a short circuit), and employing both insulators, an oxidation layer and epoxy, may not be feasible due to the tiny gap between the elements. The coil-type coaxial thermocouple proposed by Park et al. (2024) has an internal element coated with both an oxide layer and epoxy. As the outer element is formed by spooling a wire over this insulated internal piece, the difficulty of assembly is resolved, and no drilling is required. However, the size of the surface junctions directly impacts the response time; the smaller the insulation layer, the smaller junctions are required to bridge this. Therefore, it is beneficial to maintain as small a gap between the elements as possible; hence, employing one kind of insulation is more adequate.

The small dimensions of the thermocouple components require high precision to ensure a functional assembly. This can be simplified by choosing adequate geometrical and dimensional tolerances. Ideally, after assembling the thermocouple components, the insulator layer is intact, so there is no electric contact between the elements. The fitting of the sensor components can be supervised by measuring the electrical resistance between the inner and the outer parts. The aim is to have electrical resistance between the elements in the order of magnitude of megaohms. If the resistance is too low, the ends of the sensors can be visually inspected by a microscope and in the case of finding a contact point the surface has to be polished.

2.4. Extension cables

To measure the voltage output of the sensor, extension cables must be connected to the elements. The best way of this elongation in order to avoid the production of additional thermocouple junctions, given that reducing the risk of measurement bias caused by different connecting lead temperatures, could be the use of the same materials as the electrodes of the thermocouple and joining them with electric or laser welding. Dissimilar materials can be also used as extension wires as in Mohammed et al. (2008); Desikan et al. (2016), and the widespread assembly methods using bonding materials, e.g. soldering (Menezes and Bhat, 2010; Desikan et al., 2016) or conventional welding (Mohammed et al., 2008) can also be applied due to the law of intermediate materials (Lawton and Klingenberg, 1996).

3. The selected design

The goal of this work is to create tiny transducers that permit localized measurements; therefore, thermocouple designs in the order of D=2 mm featuring sensing elements over a d=1 mm circumference are targeted. When specifying the length of the sensor, one must account for the thermal penetration depth, which prescribes a minimum length according to the envisaged test time. This transducer is to be used in short-duration facilities, such as the VKI Longshot, where the test time is in the order of $t\approx 20-70\,\mathrm{ms}$. Considering a test duration with a larger margin of $t\approx 150\,\mathrm{ms}$, yields a required Chromel length of $L_{\mathrm{min,Chr}} \geq 3.4\,\mathrm{mm}$ and Constantan length of $L_{\mathrm{min,Cnn}} \geq 3.9\,\mathrm{mm}$. For practical reasons, a longer sensor in the order of $t\approx 10\,\mathrm{mm}$ is more desirable (which would even permit tests of $t\approx 10\,\mathrm{mm}$). Weighting the advantages of the taper-headed (Marineau and Hornung, 2009; Desikan et al., 2016) and straight (Buttsworth, 2001; Mohammed et al., 2008; Li et al., 2017) thermocouple designs, the latter was considered to be more favorable for manufacturing. Accordingly, the nominal design introduced in Fig. 2 is targeted.

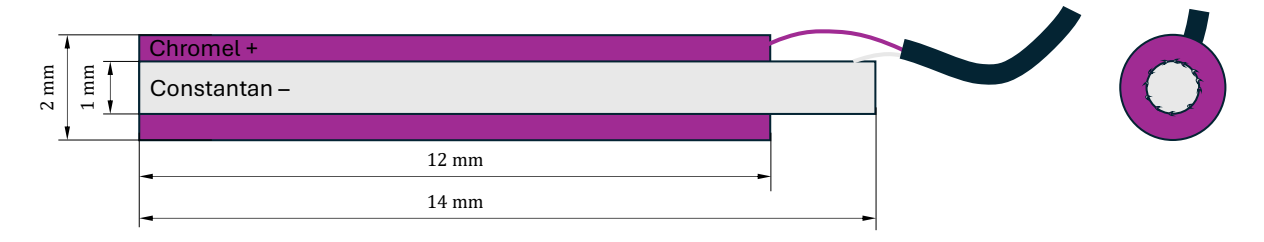


Fig 2. Schematic of coaxial thermocouple.

Regarding the insulation and assembly of the thermocouple elements, the method of Buttsworth and Jacobs (1998) is superior to the other techniques as the oxide layer formation and the fitting of the elements occur in parallel. For a specific initial radial gap, one can define the adequate oxidation parameters (temperature and exposure time) via iterations.

4. Assembly via oxide layer formation in a furnace

Buttsworth and Jacobs (1998) oxidized a K-type (Chromel–Alumel) thermocouple for 6-hours at 1000 °C

to obtain a sufficient oxide layer and bonding between the coaxially assembled elements. Kriukience and Tamulevicius (2004) investigated the oxidation of K-type thermocouples (conventional wire sensors) at temperatures of $800-900\,^{\circ}\text{C}$, and have reported that the Chromel element oxidizes approximately ten times slower than the Alumel, and found that several hours of exposure was required at $900\,^{\circ}\text{C}$ for the selective oxidation focal points to grow and join together. Regarding Constantan, Jondo et al. (2008) have demonstrated a temperature dependency in the oxidation rate of tape-like samples between $650-900\,^{\circ}\text{C}$. Oxidizing the sample at constant temperatures, they observed the process to occur over time in distinct stages. Based on the plots shown in Jondo et al. (2008), the initial rates of reactions seem to be significantly faster beyond $825\,^{\circ}\text{C}$.

Accordingly, a set of oxidation experiments was executed using a furnace in a temperature range of $650-900\,^{\circ}\text{C}$. The full procedure takes a few hours. Before the treatment, the parts are degreased and pre-assembled by hand. The ramp-up process in the furnace takes about an hour to achieve temperatures in excess of $800\,^{\circ}\text{C}$. As expected, the Constantan elements oxidized faster than Chromel; in all cases, a continuous oxide layer formed on their exterior, while the oxidation of the latter seems to have taken place in patches that have not grown together. Overall, the technique is quite promising; for several samples, both successful bonding and electrical insulation between the elements could be achieved, and the insulation could be bypassed by scratching the surface of the thermocouple. Figure 3 illustrates one of the manufactured thermocouples. The Chromel-Constantan wires have been welded to the surface of the cylindrical elements, and the spots were covered with glue. The next steps are to optimize the whole process to reduce the oxide layer thickness, which would benefit the response time.



Fig 3. Coaxial thermocouple manufactured in-house with a furnace.

5. Thermal product calibration

To evaluate the surface heat-flux from the transient temperature history measured by a coaxial thermocouple, the sensor's thermal product, β , must be known, which, as shown in Equation 1, scales the computed value. The thermal product depends on the material properties of the transducer's surface junctions. A first estimate can be obtained for β by calculating an average (even a weighting can be involved) parameter based on the individual material properties of the two metals (Mohammed et al., 2008; Desikan et al., 2016). Using Sundqvist (1992), the thermal product of Chromel and Constantan can be estimated to $\beta_{\rm Chr} = 7936\,{\rm Jm^{-2}Ks^{-1/2}}$ and $\beta_{\rm Con} = 8925\,{\rm Jm^{-2}Ks^{-1/2}}$ at $T_{\rm amb} = 293\,{\rm K}$, which deviate by $\approx 6\,\%$ from their mean. However, as shown by Buttsworth and Jacobs (1998), the value depends on the distribution of the size and material of the junctions (Chromel or Constantan in the present case), i.e., there is a dependency on how they are created; therefore, the precise assessment of the thermal product requires a sophisticated calibration. The basis of the most widely used calibration methods is the one-dimensional heat conduction theory of two semi-infinite objects. Accordingly, when two bodies of different initial temperatures ($T_{0,1}$, $T_{0,2}$) and thermal properties ($T_{0,1}$, $T_{0,2}$) and thermal properties to the thermal products of the

materials according to:

$$T_c = \frac{\beta_1 T_{0,1} + \beta_2 T_{0,2}}{\beta_1 + \beta_2} \longrightarrow \beta_1 = \beta_2 \frac{T_c - T_{0,2}}{T_{0,1} - T_c} . \tag{4}$$

Therefore, knowing the initial temperature of the objects, the material properties of one of the two, and measuring the contact temperature, allows calculating the thermal product of the other material. Such calibration can be performed by plunging a cold sensor into warm liquid (Jessen et al., 1992; Olivier and Gronig, 1995; Buttsworth and Jacobs, 1998), using a reflected shock in a shock tube (Buttsworth, 2001; Mohammed et al., 2010), or by dripping a droplet of cold liquid onto a heated sensor (Buttsworth and Jacobs, 1998; Buttsworth, 2001). Other techniques may apply radiative heat flux (Lyons and Gai, 1988; Buttsworth et al., 2005) or a comparative manner with respect to another sensor.

5.1. Experimental setup

Within these thermal product calibration methods, taking into account the instrumentation needed and the errors that may be induced, the fluid bath plunging technique and the water droplet technique seem adequate and fairly simple to implement. In this work, a water droplet-based calibration bench, similar to the one employed by Buttsworth (2001), was created and tested. The setup is illustrated in Fig. 4. To investigate the applicability and reliability of the method, the calibrations were performed on a commercial heat-flux sensor. The E-type coaxial thermocouple has sensing elements are distributed over a $D=1.0\,\mathrm{mm}$ circumference. According to the datasheet, the thermal product of this sensor is $\beta_s=8879\,\mathrm{Jm^{-2}Ks^{-1/2}}$. The thermocouple was placed into a Chromel insert, which was fitted into a thick copper plate. The temperature of the water was monitored before dripping using a K-type thermocouple. The thermocouple wire to copper wire cold junctions of both thermocouples were immersed in melting ice within an insulated box. The output of the sensors was amplified with a gain of 1000 and recorded using a Nation Instruments NI-PXI-6123 card at 500 kHz for 100 ms before and 200 ms after the droplet impact.

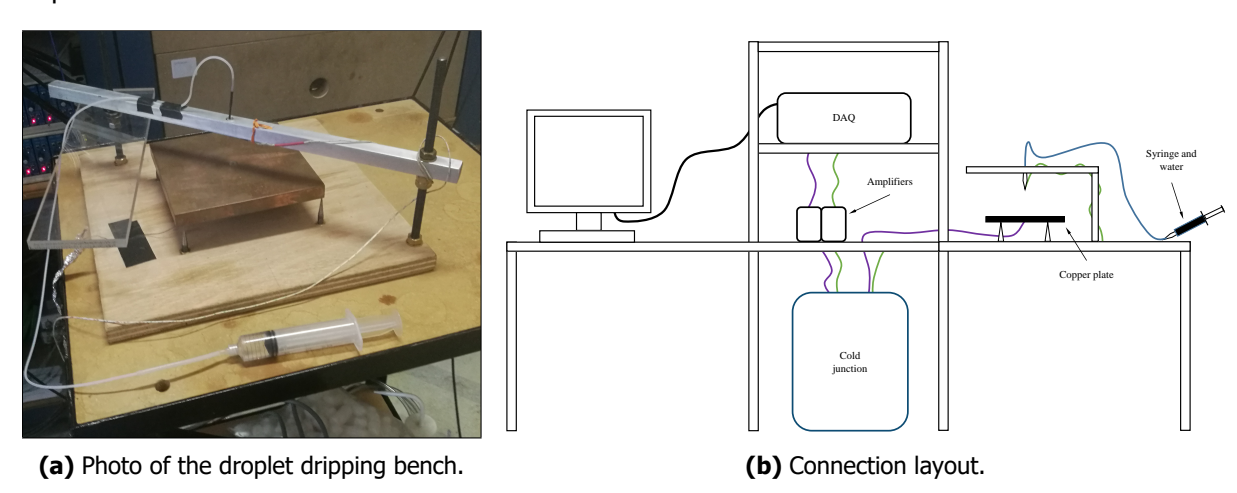


Fig 4. Schematic of thermal product calibration bench.

5.2. Parametric study on the test rig

Multiple parameters of the calibration bench have been studied to identify optimal operating conditions. Before performing each series of tests, the copper plate and the thermocouple were warmed using a heat gun, and after a short waiting period, the temperature was assumed to be homogeneous, and the tests started. The measured thermal product is evaluated using Equation 4, where the contact temperature T_c was obtained by extrapolating the post droplet impact temperature history of $t=1-5\,\mathrm{ms}$ to $t=0\,\mathrm{ms}$ (compensating for the fast, yet not instantaneous, response-time of the thermocouple).

5.2.1. Influence of the droplet height

The first parameter investigated was the height from where the water droplet is released to induce the temperature change. Figure 5 presents the comparison of measurements taken between $60\,^{\circ}\text{C} < T_s < 100\,^{\circ}\text{C}$

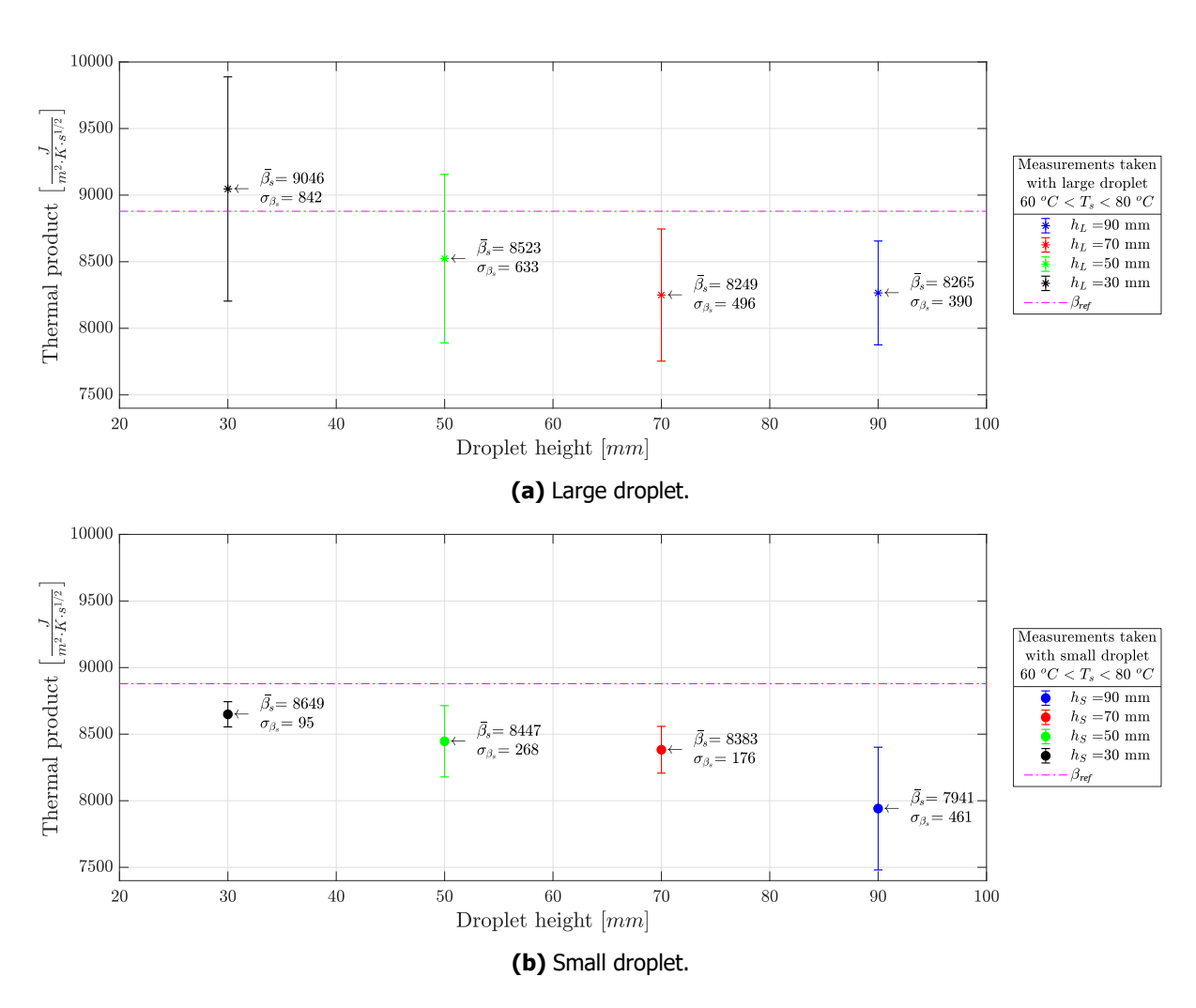


Fig 5. Influence of the water droplet height on the derivation of the thermal product.

 $80\,^{\rm o}{\rm C}$ surface temperature from different droplet heights with large and small droplets respectively. The small droplets had a size of roughly $d\approx 5\,{\rm mm}$ after the impact and remained intact, while the large droplets created rather a splash of $d\approx 15\,{\rm mm}$ over the thermocouple. Measurements were performed from the height of $h=90\,{\rm mm}$, $70\,{\rm mm}$, $50\,{\rm mm}$ and $30\,{\rm mm}$. The mean values of the measured surface thermal products $(\bar{\beta}_s)$ are presented with error bars indicating the standard deviation (σ_{β_s}) of the series of measurements. The magenta dash-dotted lines indicate the 'reference' value provided by the manufacturer of the sensor.

Fig. 5a indicates that reducing the height from which a large droplet is released leads to a thermal product closer to the reference value, although the measurement scatter significantly increases. Measurements with a small droplet demonstrate a similar converging trend in Fig. 5b, although unlike the former case, the standard deviation of the measurements reduces as the droplet height diminishes.

It must be mentioned that in the case of the $h_L=30\,\mathrm{mm}$ measurement, the mean value and the standard deviation are affected by some outliers. Moreover, approximately $10-20\,\mathrm{measurements}$ correspond to each run, except the $h_L=90\,\mathrm{mm}$ case, which was remeasured, and corresponds to $40\,\mathrm{measurements}$ (note that even with the highest number of large droplet samples, the scatter was the lowest in this case). When performing measurements, human error may also influence the results, therefore the technique has to be practiced, however, the order of performing the measurements ($h_L=70\,\mathrm{mm}$,

 $50\,\mathrm{mm}$, $30\,\mathrm{mm}$, $90\,\mathrm{mm}$ followed by small droplet tests from $h_S=90\,\mathrm{mm}$, $70\,\mathrm{mm}$, $50\,\mathrm{mm}$, $30\,\mathrm{mm}$) does not seem to influence the results. The aiming and release of a single droplet are both important and can affect the calibration. Reducing the height of the water droplet release showed a positive effect on the mean value of the calibration. This must be related to the ease of precise dripping and better repeatability at reduced distances, as targeting mistakes from higher drip heights were seen to have a higher negative impact on the results. On the other hand, at close distance, it is harder to visually notice during a test if a measurement was poorly executed. This must be identified during the data visualization, and the test must be rejected.

5.2.2. Influence of the droplet size

Figure 6 shows the temperature variation measured by the coaxial thermocouple upon the impact of the large and the small droplet from different heights. To ensure a meaningful comparison, calibrations with similar initial surface temperature were chosen. According to the visual inspection of the signals, the droplet size shows a negligible effect on the sensor output in the time range of interest $(t=0-5\,\mathrm{ms})$. Moreover, due to the fit and extrapolation applied to find the contact temperature, the effect on the surface thermal product is also minor. Based on the similarity of the signals, one can conclude that the

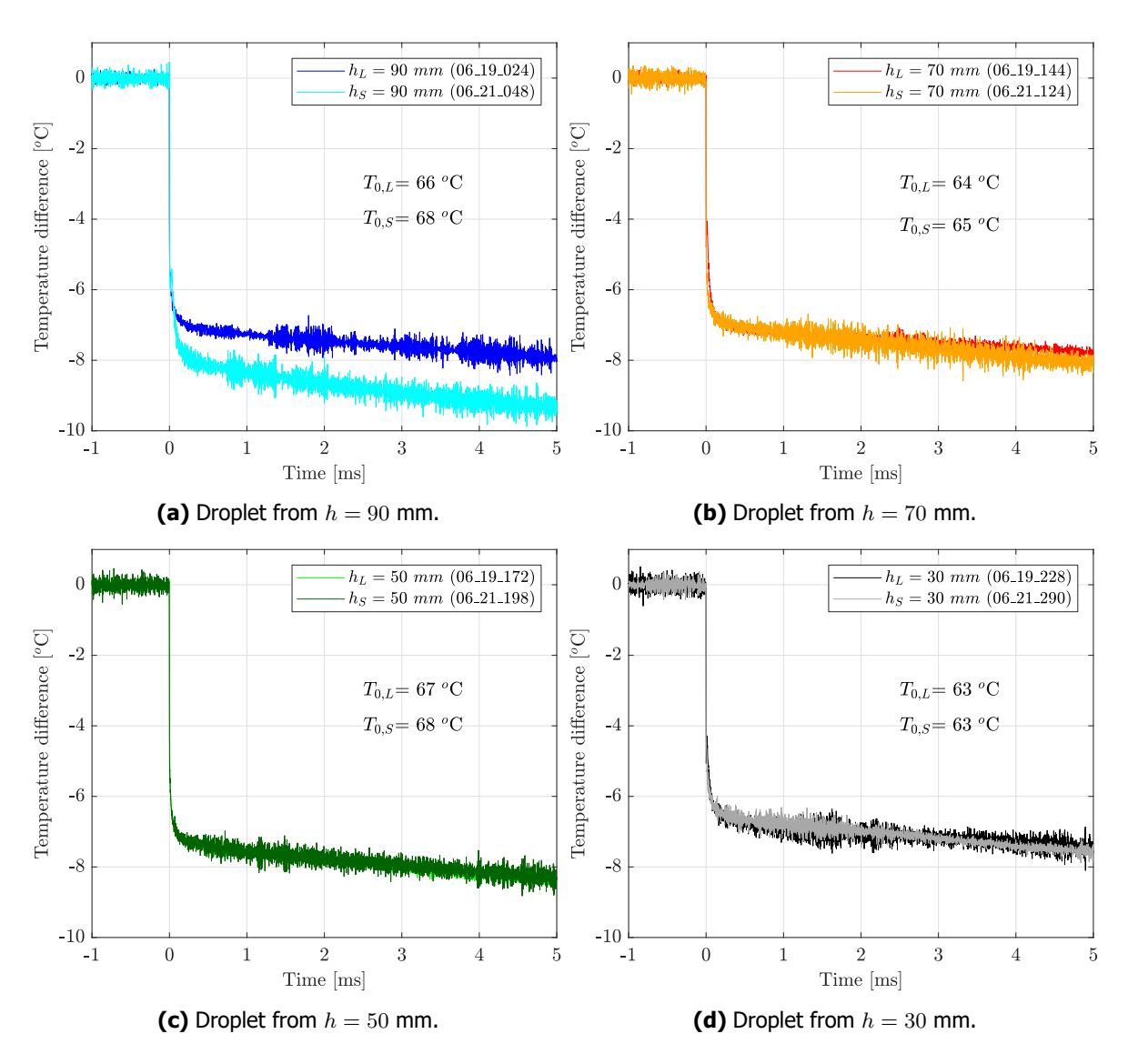


Fig 6. Influence of the droplet diameter on the temperature variation.

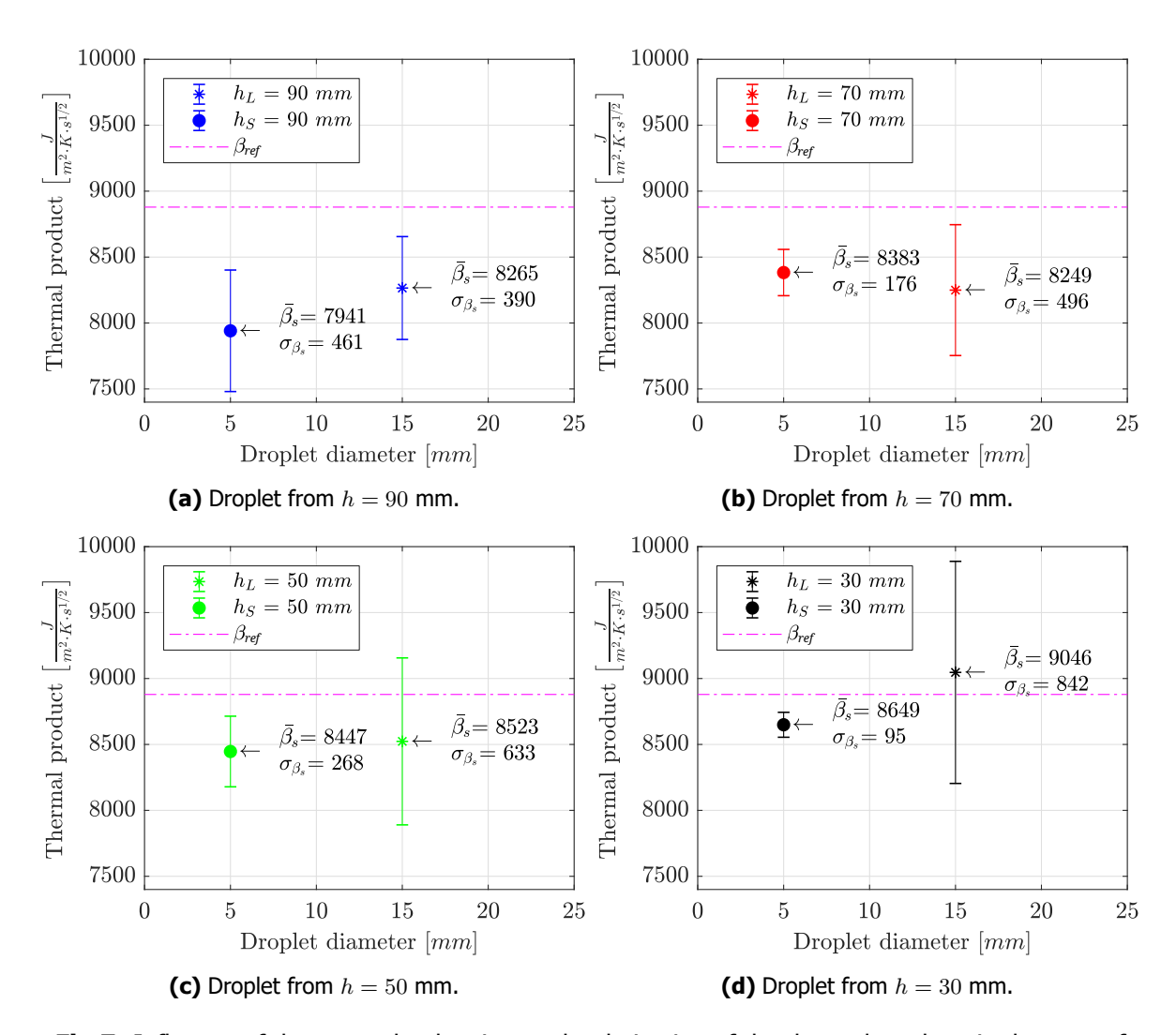


Fig 7. Influence of the water droplet size on the derivation of the thermal product, in the case of different droplet heights.

thermal effect of both droplet sizes on the surface is similar in the first few milliseconds, which suggests that the one-dimensional heat-flux assumption stands.

Observing Fig. 5 and Fig. 7, the majority of the calibration cases show that using large water droplets, the surface thermal product averages slightly closer to the datasheet value. On the other hand, this method produces greater scatter than using a small droplet. Accordingly, the repeatability of the small droplet calibrations seems to be higher, which is a major criterion. This suggests that the use of the small droplets is more beneficial.

5.2.3. Influence of the droplet viscosity

In the comparison presented in Fig. 6, only the first few milliseconds are plotted, which were used for inferring the surface thermal product. According to the first $t=5\,\mathrm{ms}$, the temperature shows a step-like change with a slope of $\partial T/\partial t \approx -0.2\,\mathrm{K/ms}$ between $t=1\,\mathrm{ms}$ and $t=5\,\mathrm{ms}$. On the longer time frame, fluctuations can be observed in the temperature signal. These are somewhat different for the two inspected droplet sizes. High-speed camera recordings illustrate in Fig. 8 the impingement of a small droplet. These confirm the correlation between the impingement and spreading-contracting motion of the droplet over the surface and the increasing-decreasing heat transfer, i.e., the recorded temperature

signal, driven by the surface tension and the viscosity of the fluid inside. Thus, one can conclude that the viscosity of the fluid affects the measured temperature variation on the millisecond time frame and suppose that it also has an impact on the initial temperature variation right after the impact.

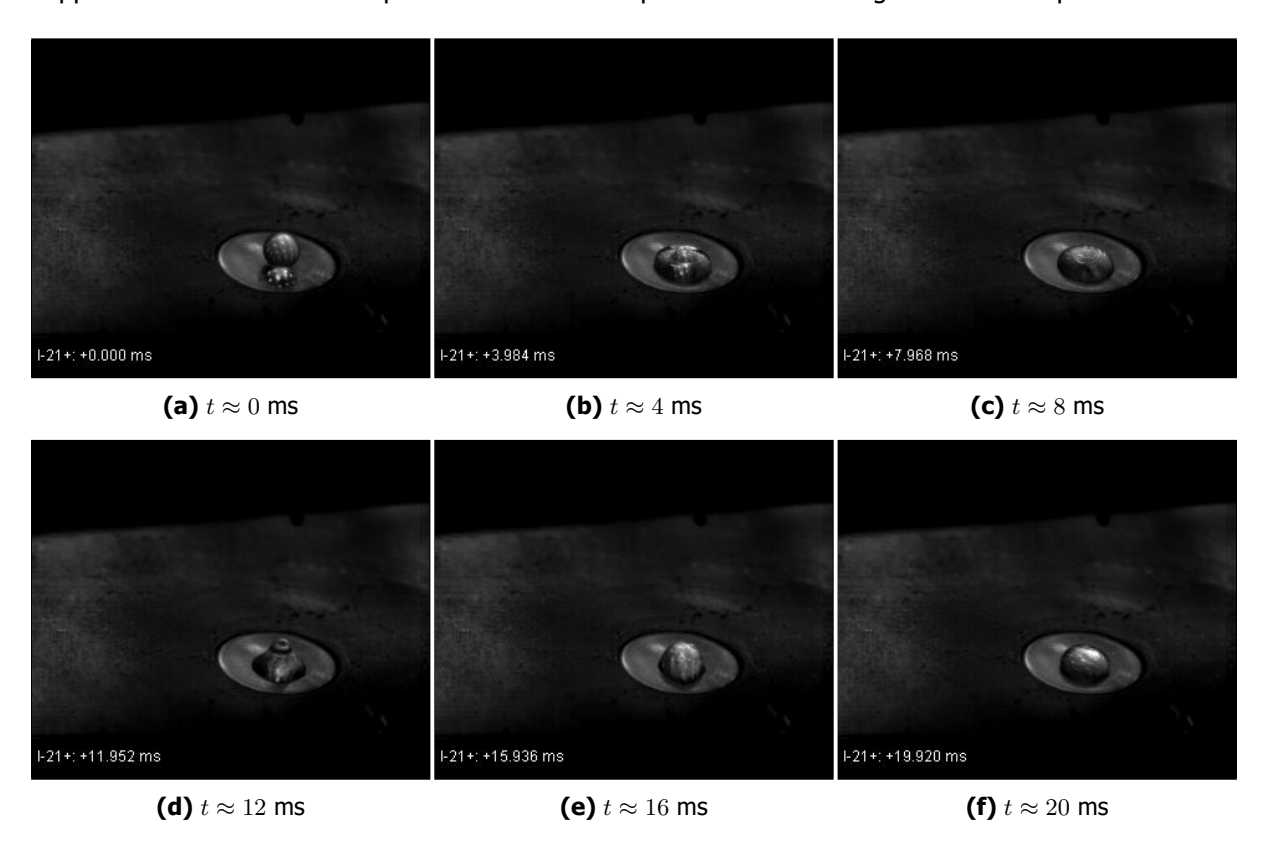


Fig 8. Direct visualization of the deformation of a water droplet upon impacting the thermocouple. The reflective surface corresponds to the Chromel insert $(D=9.3\,\mathrm{mm})$ in which the coaxial thermocouple is flush-mounted to the surface.

Experiments using Glycerol droplets

In order to investigate the effect of the viscosity inside the droplet on the calibration, measurements were taken with glycerol, which is much more viscous ($\mu_{\rm G}\approx 1.49\,{\rm Pa.s}$) at room temperature than water ($\mu_{\rm W}\approx 1.05\times 10^{-3}\,{\rm Pa.s}$). A liquid composed of $99.5\,\%$ glycerin and $0.05\,\%$ water was used. Figure 9 presents two typical temperature variations obtained with glycerol. The temperature variation is closer to the theoretical case when two semi-infinite solid bodies of different temperatures are brought into contact than in the case of the water droplet. The calibrations showed almost identical trends even in the case of different initial surface temperatures. The measured thermocouple signals can be divided into two groups; one is very close to the ideal step change, while in the other, an overshoot and a rapid convergence can be seen in the temperature variation. In a few cases, the temperature signal showed a slow convergence from above, but these tests can be neglected, assuming human error in the dripping process (such as misalignment of the dripping nozzle with respect to the sensor).

The thermal properties of glycerol were assumed to be well known; however, it was discovered during the evaluation that finding a reliable reference that also provides uncertainties for given values is cumbersome. Preliminary results on the thermal product measurement are presented in Fig. 10. These were obtained using glycerin properties noted by CAMEO Chemicals (1999), which yield for the employed temperature range $\beta_G \approx 998-991\,\mathrm{Jm^{-2}Ks^{-1/2}}$. The calibration seems to have an acceptable scatter, but a large offset can be found in between the theoretical value and the achieved results. In order to converge with the measurements, a reliable source of the thermal properties equipped with

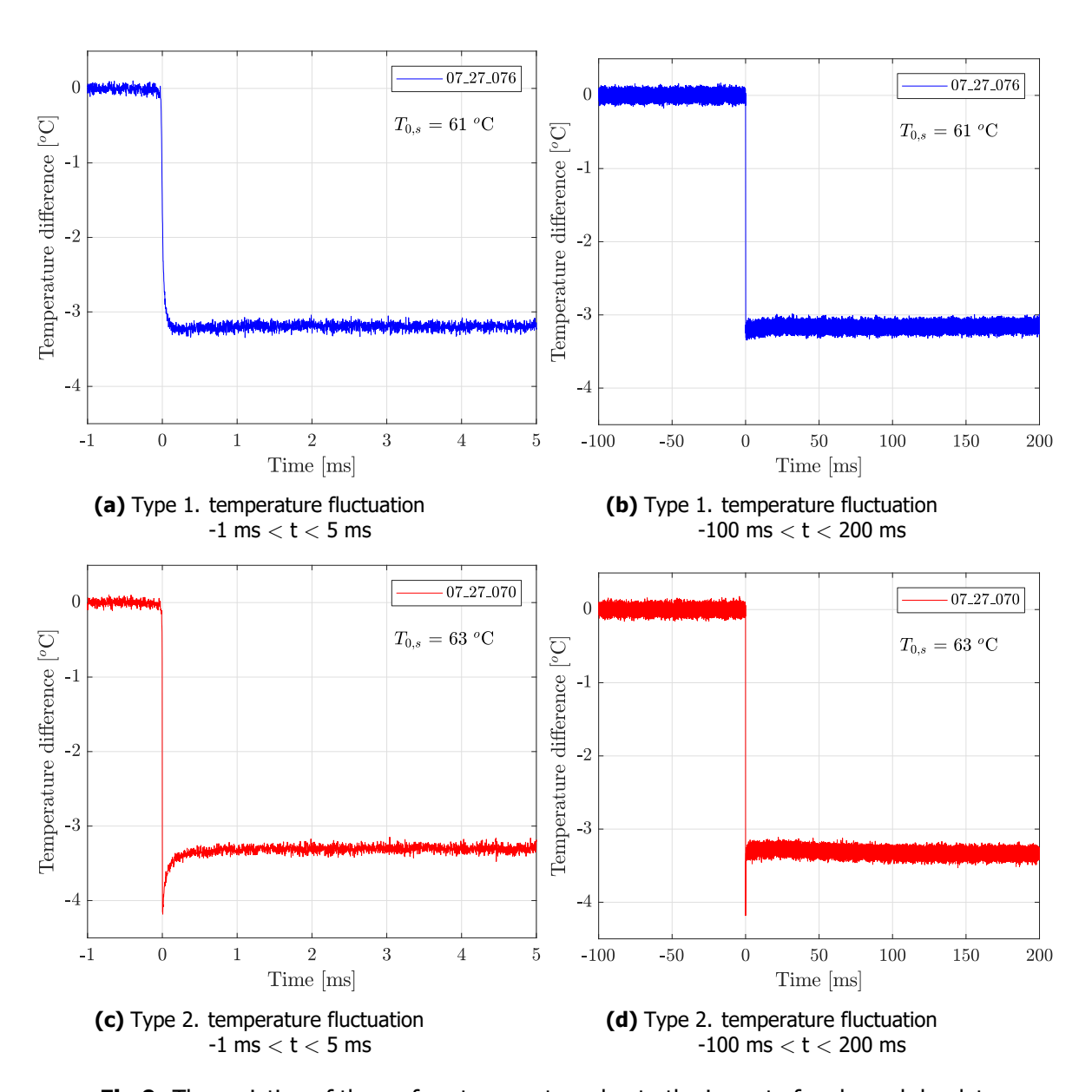


Fig 9. The variation of the surface temperature due to the impact of a glycerol droplet.

uncertainty ranges is essential.

A practical drawback of using such liquids is that the surface becomes after the calibrations oily/sticky, which is hard to clean. Since the interaction between the fluid droplet and the wetted surface is different than when it falls on a dry one (Richard and Quéré, 2000), the viscous film, left after the drying of the former droplet, may affect the surface heat-flux present during the calibration. This effect must be investigated further in future experiments.

5.2.4. Remarks on the parametric study

Collecting all the beneficial effects of the investigated parameters, near-ideal results could be achieved with the setup using a $h\approx 30\,\mathrm{mm}$ droplet height, small $(d\approx 5\,\mathrm{mm})$ distilled water droplets, employing a heat-shield between the nozzle and the sensor just until the moment of dripping. Figure 11 presents the calibration results obtained with such a configuration. The two dashed black lines separate the two measurement campaigns. The horizontal magenta line indicates the reference datasheet value of the

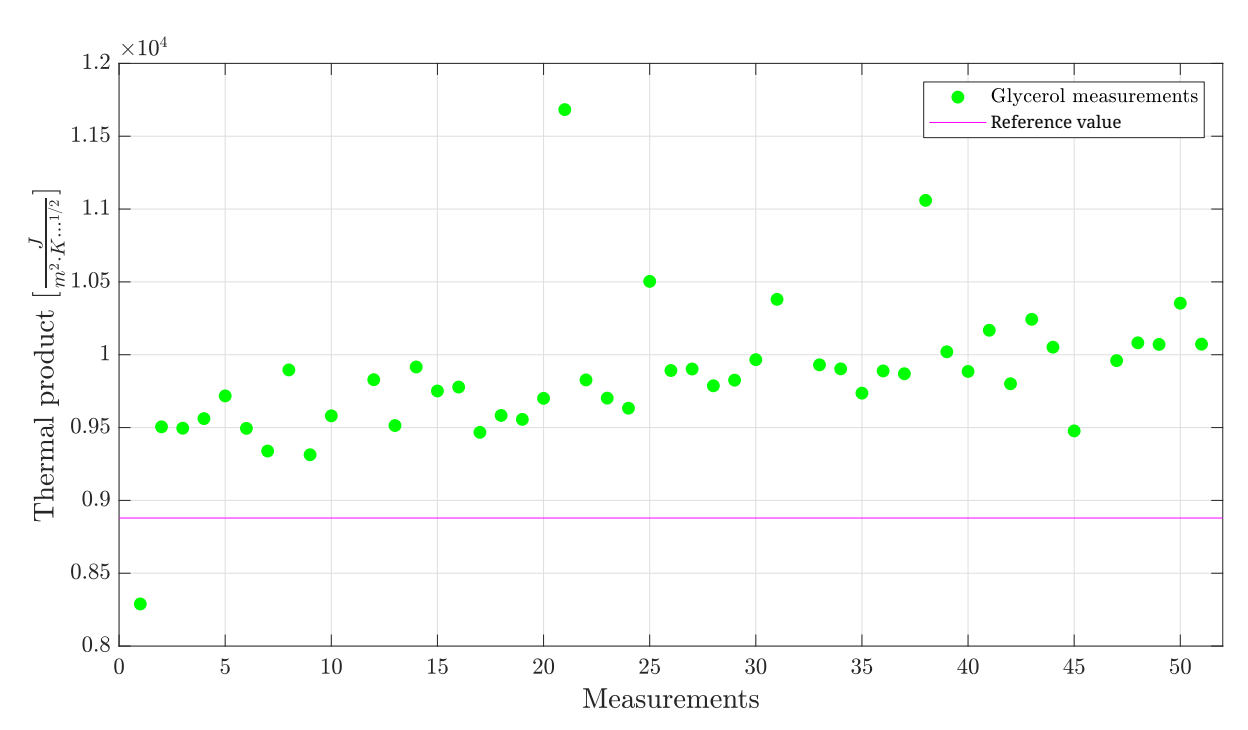


Fig 10. Scatter of the glycerin measurements.

thermal product. The dark blue and the cyan dash-dotted lines represent the theoretical thermal product

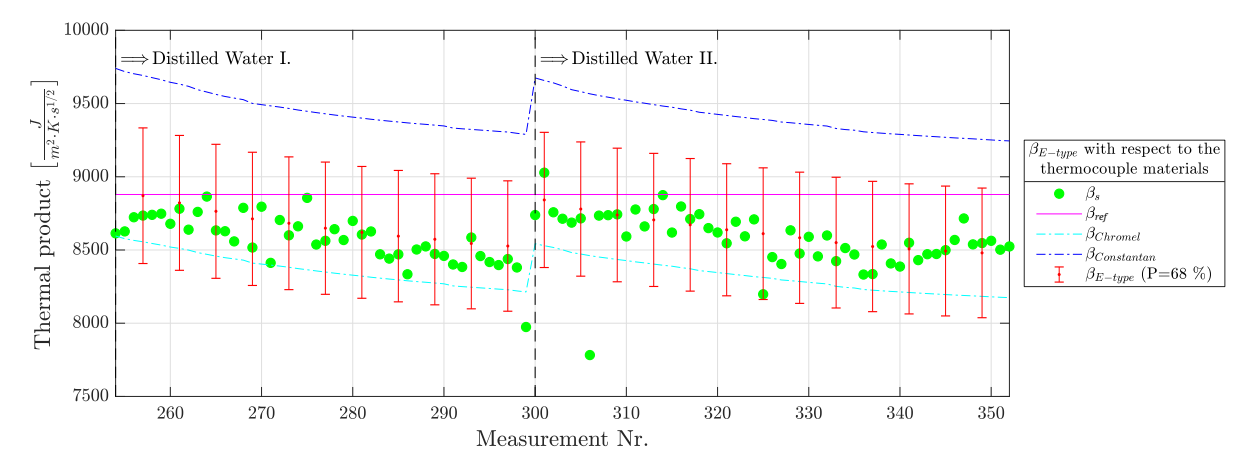


Fig 11. The variation of the thermal products measured with the application of the advantageous parameters. The sudden increase from measurement #300 corresponds to the instant the base plate was heated up again.

for the pure Constantan and the pure Chromel material respectively, which had been evaluated from the thermal diffusivity and the thermal conduction measurement results reported by Sundqvist (1992) as a function of their temperature.

During the measurements, the initially heated copper plate (and therefore the sensor) were slowly and continuously cooling. Given that, the thermal product of the individual thermocouple elements was evaluated at their actual temperature. The decaying trends reported in Fig. 11 points out a significant variation of the thermal product with the actual temperature of the sensor. The green dots represent the measured thermal product. The small red dots and their error bars indicate thermal products

for the same sensor, inferred from a weighting expressed in Eq. 5 and involving the wetted surface area of the two thermocouple elements, along with temperature dependent thermal products for each material.

$$\beta_s \approx \frac{\beta_{\rm Chr} S_{\rm Chr} + \beta_{\rm Con} S_{\rm Con}}{S_{\rm Chr} + S_{\rm Con}}$$
(5)

In conclusion, at higher surface temperatures, a fair agreement is observed between the measured thermal product and the value indicated by the datasheet of the transducer. Moreover, the measurements demonstrate an outstanding coalescence with the evaluated thermal product, following the temperature-dependent trend of the raw materials. Last but not least, almost all the measurements are covered by the uncertainties of the material properties (≈ 5 %), which indicates that the results are converging.

6. Conclusions

This paper reported on the status of the development of in-house coaxial thermocouples for transient heat-flux predictions. A miniature thermocouple design employing cylindrical components was realized. Preliminary experiments demonstrated that a furnace-based oxidation process is suitable for forming an insulation layer over the thermocouple elements and in the meantime tightly assembling them. The insulation thickness was sufficiently thin such that it could be bridged by scratching the cylindrical end of the thermocouple. Future work will focus on the optimization of the oxidation process to reduce the insulation layer's thickness, which would benefit the response time.

The second part of the paper focused on the implementation of a test bench for the calibration of the thermal product of coaxial thermocouples. A droplet dripping-based setup was created and a parametric study was executed on the bench settings using a commercial coaxial thermocouple to identify ideal usage conditions. The investigation of the droplet size, dripping height, and the effect of the fluid viscosity was presented in detail and showcased that they can influence the calibration signal and influence the scatter in the measured thermal product. The next stage of the work is going to target fine-tuning the calibration with using a viscous liquid that has well characterized thermal properties. Future investigations should focus on the determination of the thermal product and response time of the manufactured sensors. The influence of manufacturing parameters on the thickness of the oxide layer is worth being addressed, along with the potential impact it has on the response time of the thermacouple. Whether or not the method used to create the surface junction has an influence on the thermal product of the sensor or its response time should also be addressed experimentally.

Acknowledgments

This work was partially carried out under ESA contract No. 4000139380. The authors gratefully acknowledge the help of Mr. Adam Simonneau with the oxidation tests.

References

Bendersky, D. (1953). A special thermocouple for measuring transient temperatures. *Mechanical Engineering*, 2(75):117–121.

Buttsworth, D. R. (2001). Assessment of effective thermal product of surface junction thermocouples on millisecond and microsecond time scales. *Experimental Thermal and Fluid Science*, 25(6):409–420.

Buttsworth, D. R. and Jacobs, P. A. (1998). Total temperature measurements in a shock tunnel facility. In *Proceedings of the 1998 Thirteenth Australasian Fluid Mechanics Conference, Melbourne, Australia, 13-18 December 1998*, pages 51–54.

Buttsworth, D. R., Stevens, R., and Stone, C. R. (2005). Eroding ribbon thermocouples: Impulse response and transient heat flux analysis. *Measurement Science and Technology*, 16(7):1487–1494.

CAMEO Chemicals (1999). Database of Hazardous Materials, Glycerine. Technical report, National Oceanic and Atmospheric Administration, CAMEO Chemicals. https://cameochemicals.noaa.gov/chris/GCR.pdf.

- Desikan, S. L., Suresh, K., Srinivasan, K., and Raveendran, P. G. (2016). Fast response co-axial thermocouple for short duration impulse facilities. *Applied Thermal Engineering*, 96:48–56.
- Grossir, G., Pinna, F., and Chazot, O. (2019). Influence of nose-tip bluntness on conical boundary-layer instabilities at Mach 10. *AIAA Journal*, 57(9):3859–3873.
- Jessen, C., Vetter, M., and Grönig, H. (1992). Experimental studies in the Aachen hypersonic shock tunnel. *Zeitschrift für Flugwissenschaften und Weltraumforschung*, 17(2):73–81.
- Jondo, T., Galez, P., Jorda, J.-L., Le Roy, J., Marty, J., and Soubeyroux, J.-L. (2008). The oxidation mechanisms of Cu54Ni45Mn1 (constantan) tapes: Kinetic analysis. *Thermochimica acta*, 475(1-2):44–52.
- Juliano, T. J., Borg, M. P., and Schneider, S. P. (2015). Quiet tunnel measurements of HIFiRE-5 boundary-layer transition. *AIAA Journal*, 53(4):832–846.
- Kriukience, R. and Tamulevicius, S. (2004). High temperature oxidation of thin Chromel-Alumel thermocouples. *Materials Science*, 16(2):136.
- Lawton, B. and Klingenberg, G. (1996). *Transient Temperature in Engineering and Science*. Oxford University Press.
- Li, J., Chen, H., Zhang, S., Zhang, X., and Yu, H. (2017). On the response of coaxial surface thermocouples for transient aerodynamic heating measurements. *Experimental Thermal and Fluid Science*, 86:141–148.
- Lyons, P. R. A. and Gai, S. L. (1988). A method for the accurate determination of the thermal product $(\rho ck)^{1/2}$ for thin film heat transfer or surface thermocouple gauges. *Journal of Physics E: Scientific Instruments*, 21(5):445–448.
- Marineau, E. C. and Hornung, H. G. (2009). Modeling and Calibration of Fast-Response Coaxial Heat Flux Gages. *47th AIAA Aerospace Sciences Meeting*, (January):1–15.
- Menezes, V. and Bhat, S. (2010). A coaxial thermocouple for shock tunnel applications. *Review of Scientific Instruments*, 81(10):0–5.
- Mohammed, H., Salleh, H., and Yusoff, M. Z. (2008). Design and fabrication of coaxial surface junction thermocouples for transient heat transfer measurements. *International Communications in Heat and Mass Transfer*, 35(7):853–859.
- Mohammed, H. a., Salleh, H., and Yusoff, M. Z. (2010). Thermal Product of Fast Response Temperature Sensors for Transient Heat Transfer Applications with Numerically Determined Surface Heat Flux History. *The Open Thermodynamics Journal*, 4(2):36–49.
- Olivier, H. and Gronig, H. (1995). The Aachen Shock Tunnel TH2. *Zeitschrift für Flugwissenschaften und Weltraumforschung*, 1995(February 1995):73—-81.
- Park, S., Lee, H., Jang, B., Kim, J., and Park, G. (2024). Technical study of fast-response coil-type coaxial surface junction thermocouple. *Journal of Mechanical Science and Technology*, 38(3):1463–1471.
- Richard, D. and Quéré, D. (2000). Bouncing water drops. Europhysics Letters, 50(6):769-775.
- Schultz, D. and Jones, T. (1973). *Heat-Transfer Measurements in Short-Duration Hypersonic Facilities*. NATO Advisory Group for Aerospace Research and Development, Oxford.
- Sundqvist, B. (1992). Thermal diffusivity and thermal conductivity of Chromel, Alumel, and Constantan in the range 100-450 K. *Journal of Applied Physics*, 72(2):539–545.
- Surujhlal, D., Wartemann, V., and Wagner, A. (2023). Refex: Reusability flight experiment: Aerother-modynamics. In *10th EUCASS-9th CEAS Conference 2023*, pages 1–12.
- Wheaton, B. M. and Dufrene, A. T. (2024). Preflight and postflight thermal/structural analysis of BOLT II: the Holden mission. *Journal of Spacecraft and Rockets*, 61(5):1204–1218.